

# The Influence of Cr and N Additions on the Mechanical Properties of FeMnC Steels

LIEVEN BRACKE, JAN PENNING, and NURI AKDUT

The influence of Cr and N additions on the mechanical properties of austenitic Fe-Mn-Cr-C-N alloys was studied. The ductility and the strain-hardening behavior were investigated in detail, because these alloys may potentially be used for crash-relevant automotive body parts. It was found that Cr and low N additions to a Fe-18Mn-0.25C alloy resulted in a higher ductility and a reduced strain hardening. Increasing the N content up to 0.22 mass pct resulted in a further increase of ductility and a more favorable strain-hardening behavior. X-ray diffraction and transmission electron microscopy studies revealed that the strain-hardening behavior was linked to the presence of strain-induced martensite and mechanical twinning. The analysis of the mechanical properties and the microstructure clearly demonstrates that, in the Fe-Mn-Cr-C-N system, both N additions and combined N and Cr additions increase the stacking fault energy.

DOI: 10.1007/s11661-006-9084-3

© The Minerals, Metals & Materials Society and ASM International 2007

## I. INTRODUCTION

As a part of a global interest in cost-effective steel with superior strength-ductility properties, high Mn austenitic steel grades are being developed, which, in contrast to traditional austenitic steels based on the Fe-Cr-Ni alloy system, contain little or no Ni. In these alternative ferrous alloy systems, the main austenite stabilizing elements are Mn, C, and N. Most of the research in this field has been done on stainless steel grades.<sup>[1-5]</sup> For some applications, *e.g.*, structural parts in the automotive industry, the corrosion resistance is less important than the deformation behavior and Cr-free austenitic steels are actively being studied.<sup>[6,7,8]</sup> The automotive applications are mainly related to passive passenger safety systems requiring high energy absorption in the event of a crash. This requires steels with a high strength, a high ductility, and a sustained degree of strain hardening during deformation. A gradual increase of the flow stress is therefore necessary, especially at low strains in the range of what is applied during the forming operations of a structural part. In the Fe-Mn alloy system, the microstructure may contain ferrite (bcc), austenite (fcc),  $\epsilon$ -martensite (hcp), and  $\alpha'$ -martensite (bcc or bct)<sup>[9,10,11]</sup> when the Mn content is lower than 30 mass pct. In binary Fe-Mn alloys and in most high Mn (~20 mass pct Mn) ferrous alloys, the formation of  $\epsilon$ -martensite plays an essential role during plastic deformation. Because the chemical driving force  $\Delta G^{T-\epsilon}$  for the

transformation of austenite into  $\epsilon$ -martensite is proportional to the intrinsic stacking fault energy (ISFE) of the alloy,<sup>[12]</sup> it is expected that the ISFE will be the most important parameter controlling the transformation behavior of unstable austenitic steels. Several studies relate the occurrence of strain-induced austenite to  $\epsilon$ -martensite to a low ISFE in austenitic steels. According to Allain *et al.*,<sup>[13]</sup> increasing the ISFE leads to a transition from  $\epsilon$ -martensite formation to microtwinning during plastic deformation. Their results indicate that strain-induced  $\epsilon$ -martensite can be formed when the ISFE is lower than 18 mJm<sup>-2</sup> and that mechanical microtwinning can occur for ISFE values between 12 and 35 mJm<sup>-2</sup>, which confirmed earlier results by Schumann.<sup>[14]</sup> Sato *et al.*<sup>[15]</sup> report that alloys with an ISFE lower than approximately 20 mJm<sup>-2</sup> will transform into  $\epsilon$ -martensite during plastic deformation, while alloys with higher ISFE will form deformation microtwins.

The ISFE is strongly affected by the chemical composition of the alloy. In the present work, the influence of N and that of combined N and Cr additions are investigated. Several authors<sup>[16,17]</sup> report a decrease in ISFE with increasing N levels, *e.g.*, References 16 and 17. Kireeva *et al.*<sup>[16]</sup> studied the effect of N additions to an Fe-26Cr-32Ni-3Mo alloy and found that additions of 0.3 and 0.7 mass pct N reduced the ISFE from 62 to 38 mJm<sup>-2</sup> and 17 mJm<sup>-2</sup>, respectively. Stoltz *et al.*<sup>[17]</sup> added N in several amounts to low C Fe-9Mn-19Cr-7.5Ni austenitic alloys. Their results show a steep decrease of the ISFE from 53 to 33 mJm<sup>-2</sup> when adding 0.21 mass pct N and 0.24 mass pct N. Further increasing the N content did not influence the ISFE significantly.

Other authors<sup>[18-21]</sup> found an increased ISFE with increasing N content. Yakubtsov *et al.*<sup>[18,19]</sup> determined the stacking fault probability (SFP) for an Fe-8Mn-18Cr-10Ni alloy. They found that the SFP dropped from 0.0125 to 0.0055 when 0.15 mass pct N was added.

L. BRACKE, Researcher, formerly with the Department of Metallurgy and Materials Science, Ghent University, is with the Corus Research Department, NL-1970 CA, IJmuiden, The Netherlands. J. PENNING, Professor, is with the Laboratory for Iron and Steelmaking, Department of Metallurgy and Materials Science, Ghent University, B-9052, Zwijnaarde, Belgium. Contact e-mail: Jan.Penning@UGent.be. N. AKDUT is with the OCAS, Arcelor Industry Research Center, B-9060, Zelzate, Belgium.

Manuscript submitted June 7, 2006.

Article published online April 13, 2007.

Because the SFP is inversely proportional to the ISFE,<sup>[23]</sup> the addition of 0.15 mass pct N increased the ISFE. Further adding N up to 0.33 mass pct leads to an increase in SFP to 0.028, corresponding to a decreased ISFE. Karaman *et al.*<sup>[20]</sup> and Gavriljuk *et al.*<sup>[21]</sup> found that, in a Fe-24Mn-6Si-5Cr shape memory alloy, the ISFE increased when N was added up to 0.4 mass pct. Wan *et al.*<sup>[22]</sup> calculated that the ISFE increases when maximum 0.25 mass pct of N is added.

From this discussion, it is obvious that the effect of N depends on the amount added and on the other alloying elements present. For lower N levels, the ISFE increases, while for higher ones, the ISFE decreases.

Gavriljuk *et al.*<sup>[24]</sup> compared the influence of N additions with that of C additions. They added 0.4 mass pct of N and C, respectively, to an Fe-9.6Mn-18.5Cr-16.3Ni alloy and found that the N added alloy had an ISFE of 73 mJm<sup>-2</sup>, while the C added alloy had an ISFE of 37 mJm<sup>-2</sup>, clearly indicating that N more strongly increased the ISFE than did C.

Cr increases the solubility of N in the steel, as does Mn. High N steels therefore always have appreciable Cr or Mn contents. In Fe-Cr-Ni base austenitic alloys, Cr lowers the ISFE when its level is lower than 20 mass pct (Eq. [1]).<sup>[25]</sup>

$$\text{ISFE}(\text{mJ}/\text{m}^2) = 17.0 + 2.29\text{Ni} - 0.9\text{Cr} \quad [1]$$

For alloys with a higher Cr content, the ISFE can be calculated by Eq. [2].<sup>[25]</sup>

$$\text{ISFE}(\text{mJ}/\text{m}^2) = -26.6 + 0.73\text{Ni} + 2.26\text{Cr} \quad [2]$$

In the case of Fe-18Cr-9Ni steels with significant amounts of Mn and Si, the ISFE is given by Eq. [3].<sup>[25]</sup>

$$\text{ISFE}(\text{mJ}/\text{m}^2) = 1.2 + 1.4\text{Ni} + 0.6\text{Cr} + 17.7\text{Mn} - 44.7\text{Si} \quad [3]$$

Schramm and Reed<sup>[26]</sup> investigated the influence of low quantities of C, N, Si, and Mn on the ISFE in the Fe-Cr-Ni system, with Cr and Ni contents, respectively, ranging from 8.5 to 30 pct, and from 9.43 to 24.7 pct. They report the following expressions [4a] through [4d] for the ISFE:

$$\text{ISFE}(\text{mJm}^{-2}) = 4 + 1.8\text{Ni} - 0.2\text{Cr} + 410\text{C} \quad [4a]$$

C : 0.012 to 0.027 pct

$$\text{ISFE}(\text{mJm}^{-2}) = 34 + 1.4\text{Ni} - 1.1\text{Cr} - 77\text{N} \quad [4b]$$

N : 0.004% to 0.044 pct

$$\text{ISFE}(\text{mJm}^{-2}) = 34 + 2.2\text{Ni} - 1.1\text{Cr} - 13\text{Si} \quad [4c]$$

Si : 0.01 to 0.59 pct

$$\text{ISFE}(\text{mJm}^{-2}) = 32 + 2.4\text{Ni} - 1.2\text{Cr} - 1.2\text{Mn} \quad [4d]$$

Mn : 0.001 to 1.56 pct

Jiang *et al.*<sup>[23]</sup> found an increase in ISFE when Cr and N were simultaneously added to an Fe-Si-Mn-based shape memory alloy.

From the previous discussion, it is clear that the influence of a specific alloying element on the ISFE depends on the presence of the other alloying additions and that therefore one needs to be alert when assumptions are made about the influence of a specific alloying element on the ISFE.

The ISFE is not only important for the transformation behavior; it also has a pronounced influence on the strain-hardening behavior. A lower ISFE results in more planar slip because the wider stacking faults make cross-slip more difficult. If no strain-induced transformation or twinning occurs, this results in a higher strain-hardening rate.

The presence of N in austenitic steel grades strongly influences the strength of these alloys. N acts as a strong interstitial hardener of the austenitic phase.<sup>[27-30]</sup> The increased strength should also interfere with the transformation from austenite to  $\alpha'$  martensite, because this transformation is associated with a rather large volume change requiring the plastic deformation of the parent austenite phase. The N is also expected to increase the ductility.<sup>[27,30]</sup> Gavriljuk<sup>[32]</sup> and Gavriljuk *et al.*<sup>[33]</sup> attribute the increased ductility of high N steels to an increased metallic component of the interatomic bonds in alloys containing up to 0.4 mass pct N. For higher N contents, Gavriljuk<sup>[32]</sup> reports an increased covalent contribution to the interatomic bonds, resulting in a lower ductility.

The aim of this work was the development of a new cost-effective austenitic steel, based on the Fe-Mn-C alloying system, with excellent strength and strain-hardening properties, resulting in a ductile material that can be used for safety parts in the automotive industry. These properties can be achieved through a careful control of the strain-induced formation of martensite and of the mechanical twinning.<sup>[34,35,36]</sup> Both are mainly controlled by the ISFE of the alloy.

Special interest is paid to the addition of N, because this element has an important influence on the ISFE and is expected to enhance strength and ductility. To increase the solubility of N, Cr had to be added as well. As a consequence, the properties of the alloys studied reflect the influence of both N and Cr.

A solid-state annealing in a N<sub>2</sub> atmosphere was performed to further increase the N content in order to achieve even better mechanical properties.

## II. EXPERIMENTAL

The chemical compositions of three Fe-Mn-C alloys used for the present work are given in Table I. The main compositional parameters are the Cr content, which was in the range of 5.6 to 9.7 mass pct, and the N content, which was in the range of 0.114 to 0.196 mass pct. Table I illustrates the effectiveness of Cr additions in increasing the alloy nitrogen content.

The alloys were laboratory cast and rough rolled to a thickness of 25 mm prior to reheating to 1250 °C before finishing hot rolling. The hot rolling process consisted of five passes in order to obtain a final thickness of 3 mm. The finishing temperature was always kept higher than 950 °C. The rolled strip was slowly cooled from 650 °C to room temperature during 12 hours. After hot rolling, each alloy was annealed at 1050 °C for 15 minutes and water quenched to room temperature.

In order to obtain a higher N content in the low Cr and med Cr alloys, an additional annealing treatment in a N<sub>2</sub> atmosphere was carried out in order to introduce supplementary N into solid solution in the austenite phase by diffusion.<sup>[37]</sup> For this annealing treatment, as-rolled material was used. First, the samples were annealed at 850 °C for 15 minutes under a H<sub>2</sub> atmosphere of 1013 hPa to reduce oxides. This annealing treatment was followed by annealing at 1100 °C for 3 hours in a 2026 hPa N<sub>2</sub> atmosphere. The N contents are presented in Table I, for the hot-rolled and annealed samples (N<sub>HRA</sub>) and for the samples annealed in the N<sub>2</sub> atmosphere (N<sub>N<sub>2</sub></sub>). A Spectra GDA-750 glow discharge optical emission spectrometer (GDOES) operated in DC mode at 1000 V and 25 mA was used to qualitatively study the concentration profiles. It was found that the N content close to the surface was about 45 pct higher than in the center of the samples, so the N was not homogeneously distributed through the thickness of the material. It is assumed that the bulk concentration, as determined by the fusion method and listed in Table I, corresponds to the value at one-quarter of the thickness under the surface. This, in a first approximation, implies a linear concentration gradient, because the annealing time was not sufficient to reach a full equilibrium in the samples. This is directly due to the too high sample thickness.

Room-temperature tensile tests were carried out on test bars with a width of 12.5 mm and a gage length of 50 mm. The strain rate applied was  $16.7 \times 10^{-3} \text{ s}^{-1}$  for deformation up to 2 pct. From a strain of 2 pct, the rate was increased to  $20 \times 10^{-2} \text{ s}^{-1}$ .

**Table I. Chemical Composition of the Ferrous Alloys Used in the Present Study in Mass Percent**

| Alloy   | Mn   | Cr  | C    | Si   | N <sub>HRA</sub> * | N <sub>N<sub>2</sub></sub> ** |
|---------|------|-----|------|------|--------------------|-------------------------------|
| Low Cr  | 16.2 | 5.6 | 0.25 | 0.14 | 0.114              | 0.163                         |
| Med Cr  | 19   | 7.7 | 0.24 | 0.23 | 0.157              | 0.196                         |
| High Cr | 19   | 9.7 | 0.24 | 0.24 | 0.196              | —                             |

\*N<sub>HRA</sub> is the N content in the hot rolled and annealed condition.

\*\* N<sub>N<sub>2</sub></sub> is the N content in the N<sub>2</sub>-atmosphere annealed condition.

The X-ray diffraction (XRD) measurements were carried out by means of a Siemens (Munich, Germany) 5000 diffractometer, using Mo K<sub>α</sub> radiation ( $\lambda = 0.070926 \text{ nm}$ ). Samples were taken at one-quarter of the total thickness. This was done to eliminate surface effects and, in the case of the samples annealed in N<sub>2</sub> atmosphere, to link the phases present in the deformed microstructures with the bulk N concentration, eliminating the effect of the N concentration gradient. Phase determination was done using the direct comparison method.<sup>[38]</sup> The fraction of  $\alpha'$ -martensite in the different materials was determined by magnetic saturation measurements.

Thin foil transmission electron microscopy (TEM) analysis was done on a PHILIPS\* EM420, operated at

---

\*PHILIPS is a trademark of Philips Electronic Instruments Corp., Mahwah, NJ.

---

120 kV. The thin foils were prepared by electrolytical double-jet polishing using a solution of 5 pct HClO<sub>4</sub> + 95 pct CH<sub>3</sub>OOH at a temperature of 13 °C. The voltage applied was 45 V.

The ISFE of the low Cr and the high Cr alloys was determined by measuring the distance between the partial dislocations binding the stacking fault, based on weak beam dark-field TEM images. The following expression was used:<sup>[39]</sup>

$$d = \frac{Gb_1b_2}{8\pi\text{ISFE}} \cdot \frac{(2-\nu)}{(1-\nu)} \cdot \left(1 - \frac{2\nu \cos 2\alpha}{2-\nu}\right) \quad [5]$$

where

$d$  = the distance between the partials binding the ISFE (m),

$G$  = the shear modulus (Pa),

$b_1$  and  $b_2$  = the size of the Burgers vectors of the two partials (m),

$\nu$  = the Poisson's ratio, and

$\alpha$  = angle between the Burgers vector of the undissociated dislocation and the dislocation line (deg).

The sample preparation for light optical metallography consisted of mechanical polishing, electrolytical polishing (solution: 90 mL distilled water, 730 mL ethanol, 100 mL butylcellosolve, 78 mL perchloric acid), and etching (aqueous solution: 1.2 pct K<sub>2</sub>S<sub>2</sub>O<sub>5</sub>, 0.5 pct NH<sub>4</sub>HF<sub>2</sub>).

## III. RESULTS

### A. Optical Metallography

Figure 1 shows light optical micrographs of the different alloys in the hot-rolled and annealed and the N<sub>2</sub> annealed conditions. All alloys possess a fully austenitic microstructure. The grain sizes are given in Table II. The med Cr and high Cr alloys in the hot-rolled and annealed condition have smaller grains than the low Cr alloy. Also note that the grain sizes for the N<sub>2</sub>

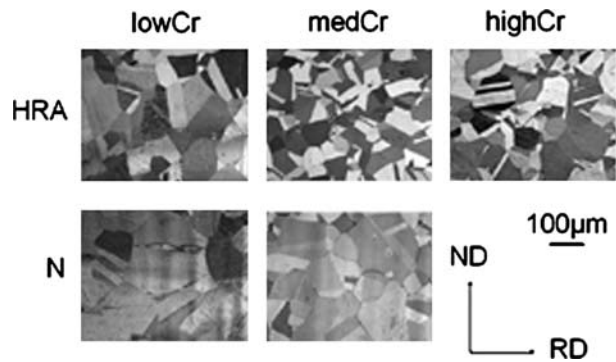


Fig. 1—Light optical micrographs of the samples studied (etchant: aqueous solution of 1.2 pct  $K_2S_2O_5$ , 0.5 pct  $NH_4HF_2$ ).

annealed samples are larger than for the corresponding hot-rolled and annealed condition.

## B. Mechanical Properties

### 1. Hot-rolled and annealed condition

Table II lists the mechanical properties of the different alloys in the two different conditions. When the properties of the hot-rolled and annealed samples of the different alloys are compared, the effect of alloying with Cr and low N levels becomes evident. The low yield strength ( $R_{p0.2}$ ) of the low Cr alloy is due to the lower amount of alloying elements as compared to the other alloys. Mainly, the lower N content of the low Cr alloy significantly reduces the yield strength.

The uniform elongation for the low Cr alloy is equal to the total elongation. The absence of a reduction of area is an indication of a more brittle fracture mode than in the case of the med Cr and the high Cr alloys. The addition of Cr and N clearly resulted in a large increase in elongation, which is proof of an increased formability and a higher energy absorption potential. Incremental strain-hardening data ( $n_i$ ) are presented in Figure 2. Table II gives mean values for the strain-hardening coefficient in the range of 1 to 5 pct tensile strain ( $n_{1-5 \text{ pct}}$ ) and in the range of 10 to 20 pct tensile strain ( $n_{10-20 \text{ pct}}$ ). From these data, it is clear that the low Cr alloy had a very high strain-hardening rate in the initial stages of deformation, while the high Cr alloy had a lower one. The med Cr alloy had an intermediate strain-hardening value. The more gradual increase in strain hardening of the high Cr alloy, in particular, is beneficial in relation to its potential use as a crash-resistant alloy in automotive applications. The high value of the strain-hardening coefficient was found to be related to the strain-induced transformation of austenite

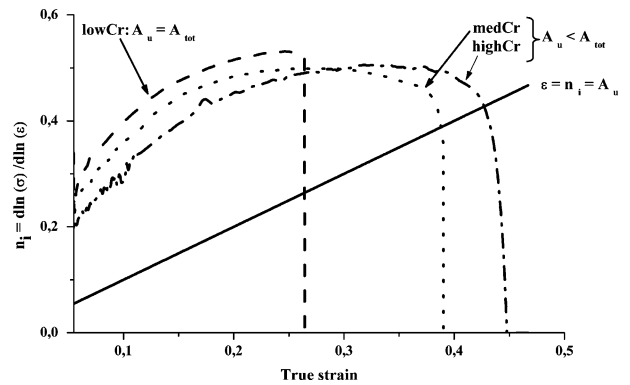


Fig. 2—Incremental strain-hardening coefficient of the alloys tested in tension in the hot-rolled annealed condition. The line  $n_i = \epsilon$  corresponds to the Considère criterion, indicating uniform elongation.

into  $\epsilon$ -martensite or into  $\alpha'$ -martensite, as will be discussed in Section C. The high fraction of strain-induced  $\epsilon$ - and  $\alpha'$ -martensite was also responsible for the high tensile strength ( $R_m$ ) and the low elongation of the low Cr alloy.

### 2. Annealing in a $N_2$ atmosphere

Figure 3 shows the true stress-true strain curves and the incremental strain-hardening value ( $n_i$ ) for the low Cr and med Cr alloys in the hot-rolled and annealed condition and in the  $N_2$  annealed condition. It is clear from this graph that adding N reduced strain hardening. The value of strain hardening at the start of deformation was not strongly influenced by N in the case of the med Cr alloy, as can be seen in Figure 3(b) and from the average value for the strain-hardening coefficient between 1 and 5 pct strain,  $n_{1-5 \text{ pct}}$ , listed in Table II. The influence of N on the initial stages of deformation in the case of the low Cr alloy was more pronounced: the addition of N markedly reduced the strain-hardening rate, as can be clearly seen in Figure 3(a) and Table II.

The N alloying resulted in an increased 0.2 pct proof stress, as can be seen in Figure 3 and Figure 4, the latter containing data of the present work together with data presented by some of the current authors in a previous publication<sup>[41]</sup> and other literature data.<sup>[27-30]</sup>

## C. Phase Analysis

### 1. Hot-rolled and annealed condition

Table III shows the results of the XRD and MSM phase analysis obtained after tensile testing to fracture. It should be noted that the amount of  $\epsilon$ -martensite present in the material was difficult to determine directly

Table II. Grain Sizes and Mechanical Properties, Engineering Values

| Alloy   | Condition             | Grain Size ( $\mu m$ ) | $R_{p0.2}$ (MPa) | $R_m$ (MPa) | $A_u$ (Pct) | $A_{tot}$ (Pct) | $n_{1-5}$ (Pct) | $n_{10-20}$ (Pct) |
|---------|-----------------------|------------------------|------------------|-------------|-------------|-----------------|-----------------|-------------------|
| Low Cr  | hot rolled + annealed | 49                     | 240              | 848         | 31          | 31              | 0.301           | 0.498             |
| Low Cr  | $N_2$ annealed        | 60                     | 338              | 761         | 36          | 36              | 0.179           | 0.451             |
| Med Cr  | hot rolled + annealed | 37                     | 317              | 779         | 47          | 51              | 0.175           | 0.449             |
| med Cr  | $N_2$ annealed        | 50                     | 328              | 741         | 56          | 59              | 0.161           | 0.396             |
| high Cr | hot rolled + annealed | 40                     | 323              | 767         | 55          | 59              | 0.145           | 0.370             |



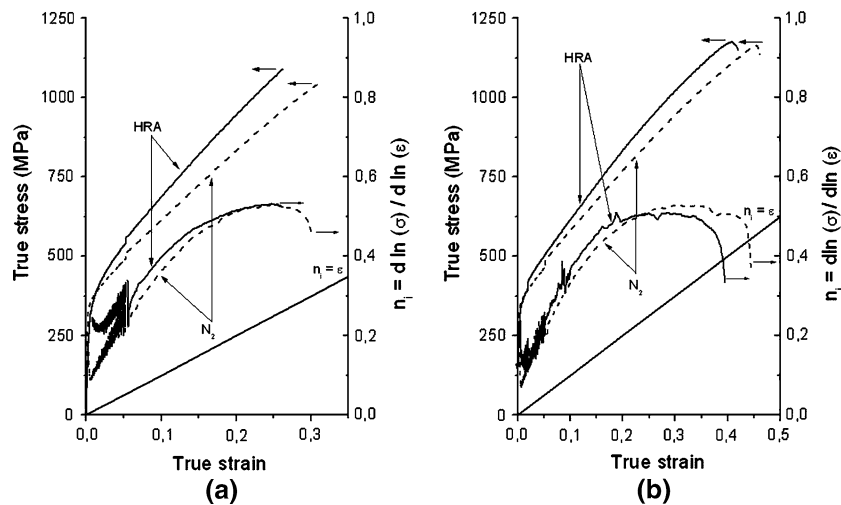


Fig. 3—True stress-true strain curves and incremental strain-hardening curves,  $n_i$ : (a) low Cr alloy and (b) med Cr alloy.

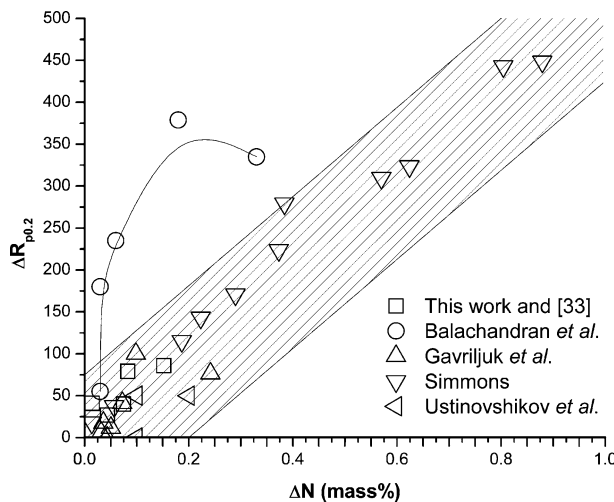


Fig. 4—Influence of N addition on the 0.2 pct proof stress: data from the current authors compared to literature data<sup>[27–30]</sup>.

by means of XRD, because many diffraction peaks of austenite,  $\alpha'$ -martensite, and  $\epsilon$ -martensite overlap and peak deconvolution is complex. Theoretical peak intensities for the different phases could not be used due to strong texture effects as a result of plastic deformation. The absolute values for the volume fractions of  $\epsilon$ -martensite therefore may not be totally correct, but

**Table III. Phase Composition after Tensile Testing (Volume Fractions)**

| Alloy   | Condition               | Austenite | $\epsilon$ -Martensite | $\alpha'$ -Martensite |
|---------|-------------------------|-----------|------------------------|-----------------------|
| Low Cr  | hot rolled + annealed   | 0.568     | 0.352                  | 0.090                 |
| Low Cr  | N <sub>2</sub> annealed | 0.870     | 0.110                  | 0.020                 |
| Med Cr  | hot rolled + annealed   | 0.874     | 0.126                  | 0                     |
| Med Cr  | N <sub>2</sub> annealed | 1         | 0                      | 0                     |
| High Cr | hot rolled + annealed   | 1         | 0                      | 0                     |

the tendencies certainly are, as the same peak analysis procedure was used for all the samples.

At 5 pct of tensile strain, no  $\epsilon$ - or  $\alpha'$ -martensite could be detected in the med Cr and high Cr alloys. In the case of the low Cr alloy, 6.5 pct  $\epsilon$ -martensite and 1.2 pct  $\alpha'$ -martensite were found.

After tensile testing, the low Cr alloy revealed the presence of a high fraction of  $\epsilon$ -martensite and  $\alpha'$ -martensite. Figure 5 shows a TEM micrograph illustrating the presence of the three phases in the low Cr alloy. Figure 6 shows dark-field images using diffraction spots characteristic for each phase. Note that the  $\alpha'$ -martensite islands were always restricted to bands of closely spaced  $\epsilon$ -martensite plates. The observed

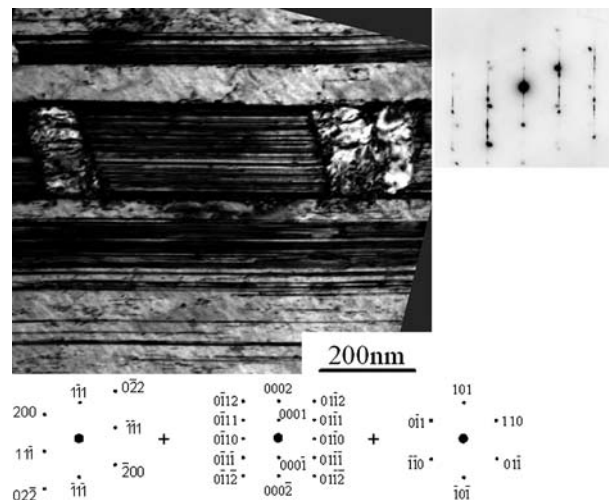


Fig. 5—Top left: TEM bright-field micrograph of the low Cr alloy, tested in tension in the hot-rolled and annealed condition. The microstructure is mainly untransformed austenite containing dense bands of  $\epsilon$ -martensite. The  $\alpha'$ -martensite is always associated with the dense bands of  $\epsilon$ -martensite. Top right: corresponding electron diffraction pattern. Below: analysis of the diffraction pattern, resulting from the superposition of diffraction spots of  $\gamma$ ,  $\epsilon$ , and  $\alpha'$  when the electron beam is parallel to  $[011]_\gamma$  //  $[2110]_\epsilon$  //  $[111]_{\alpha'}$ .

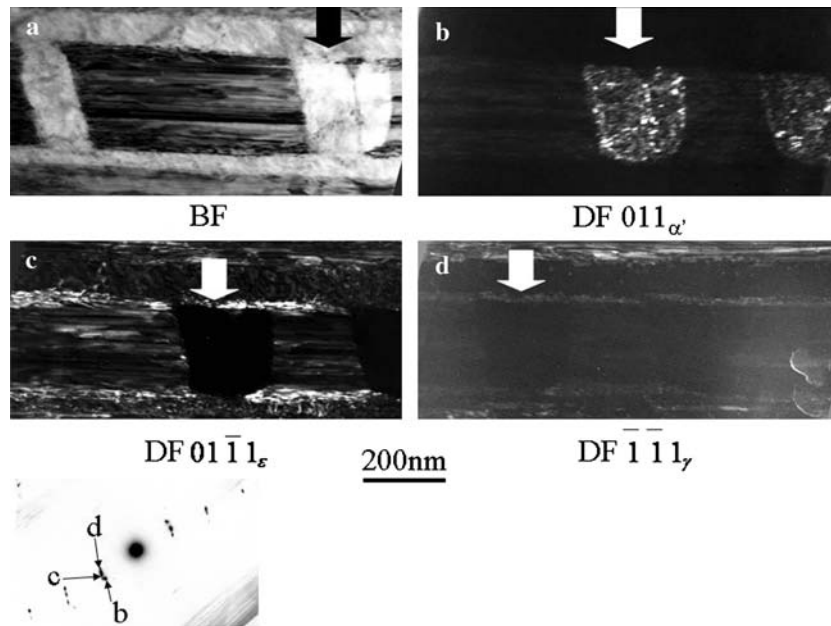


Fig. 6—TEM micrographs of the low Cr alloy, tensile tested in the hot-rolled and annealed condition: (a) bright-field image, (b) dark-field image using the  $011_{\alpha'}$  reflection, (c) dark-field image using the  $01\bar{1}1_{\epsilon}$  reflection, and (d) dark-field image using the  $\bar{1}\bar{1}1_{\gamma}$  reflection. Arrows indicate corresponding areas.

orientation relationship obeys both the expected Bogers–Burgers relationship between  $\alpha'$ -martensite and  $\epsilon$ -martensite and the Kurdjumov–Sachs relationship between  $\alpha'$ -martensite and austenite:

$$\begin{aligned} \{111\}_{\gamma} // \{110\}_{\alpha'} // \{0001\}_{\epsilon} \\ \langle 110 \rangle_{\gamma} // \langle 111 \rangle_{\alpha'} // \langle 2\bar{1}10 \rangle_{\epsilon} \end{aligned} \quad [6]$$

The med Cr alloy did not transform into  $\alpha'$ -martensite but into  $\epsilon$ -martensite. The TEM micrograph in Figure 7 also shows the presence of strain-induced microtwins in the med Cr alloy. The high Cr alloy did not contain  $\epsilon$ -martensite after fracture, but up to 10 vol pct of  $\epsilon$ -martensite was found at intermediate deformation stages. The TEM investigation revealed the presence of dense microtwins, as shown in Figure 8. Also note the formation of subcells and low-angle grain boundaries in Figure 9. From these results, it can be concluded that the addition of Cr and N ( $< 0.2$  mass pct) changes the deformation mechanism from strain-induced martensitic transformation to mechanical microtwinning. The strain-induced martensitic transformation seemed to have had a more pronounced influence on the strain-hardening behavior than mechanical twinning; the  $\gamma \rightarrow \epsilon$  transformation resulted in a higher incremental strain-hardening coefficient, which is clear when comparing Table III, which gives the phase composition, with Table II, which includes the strain hardening.

## 2. Annealing in $N_2$ atmosphere

The alloys were fully austenitic after annealing under  $N_2$  atmosphere.

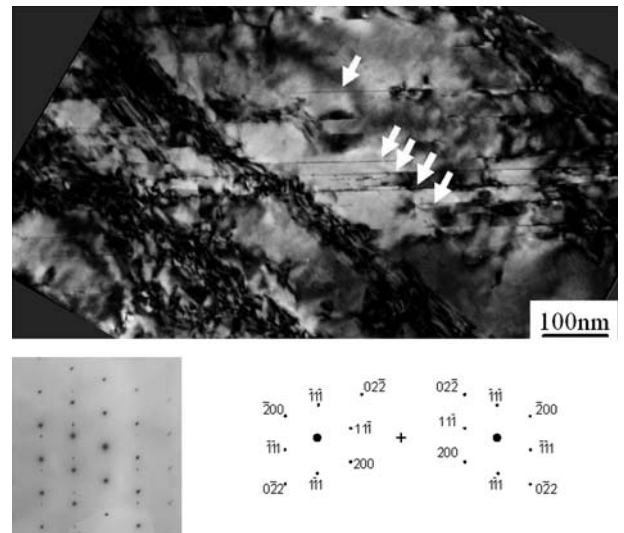


Fig. 7—TEM bright-field micrograph of the Med Cr alloy after tensile test in the hot-rolled and annealed condition showing the presence of microtwins (indicated by the arrows). Electron beam  $// [011]_{\gamma}$ .

The low Cr alloy contained less strain-induced  $\epsilon$ - and  $\alpha'$ -martensite in the  $N_2$  annealed condition than in the hot-rolled and annealed one after tensile testing (Table - III). This was expected on the basis of the lower strain-hardening coefficient observed earlier. The  $N_2$  annealed sample of the low Cr alloy also contained dense bands of microtwins, as shown in Figure 10. The med Cr alloy did not undergo any phase transformation after annealing in  $N_2$  atmosphere. For this alloy, the strain-hardening

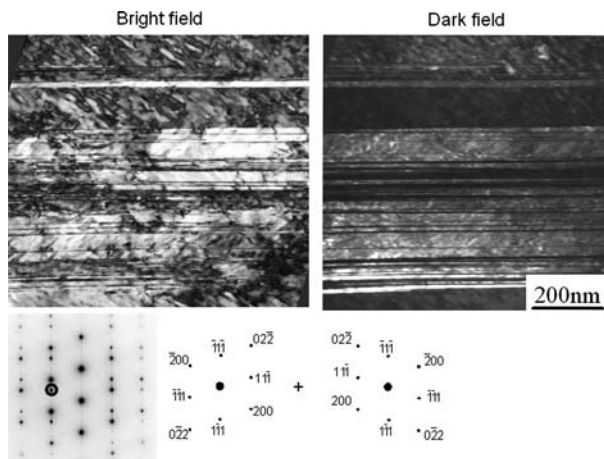


Fig. 8—TEM micrographs of the high Cr alloy, tested in tension in the hot-rolled and annealed condition. Left: bright-field micrograph of a region with microtwins. Right: same region observed in the dark field using the 200 reflection of one of the twins. Below: electron diffraction pattern, with analysis proving the twin structure, electron beam // [011].

coefficient was found to be lower for the N<sub>2</sub> annealed sample than for the hot-rolled and annealed sample. It is very probable that this alloy deformed by mechanical twinning, because these were already found in the hot rolled and annealed sample.

Figure 11 shows that the alloys with a higher yield strength, *i.e.*, in the N<sub>2</sub> annealed condition, had less tendency to display strain-induced transformation behavior during tensile testing than the alloys with a lower yield strength, *i.e.*, in the hot-rolled and annealed condition.

#### D. ISFE Measurement

The values of the ISFE for the low Cr and high Cr alloys in the hot-rolled and annealed condition were measured to be 5 and 20 mJm<sup>-2</sup>, respectively; so the addition of Cr and N increases the ISFE.

### IV. DISCUSSION

The diffusionless martensitic transformation behavior of the ferrous alloys studied in the present work is influenced by two important parameters: the ISFE and

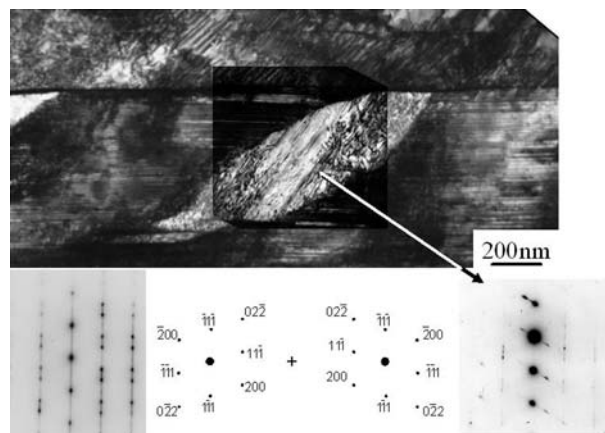


Fig. 10—Top: TEM bright-field micrograph of the low Cr alloy, tested in tension after annealing in a N<sub>2</sub> atmosphere, shows a clear intersection of two bands of microtwins. Below left: electron diffraction pattern, with analysis proving the twin structure, electron beam // [011]. Below right: electron diffraction pattern at the intersection of the twinned bands. No evidence for  $\epsilon$ -martensite or  $\alpha'$ -martensite. Electron beam // [011].

the intrinsic strength of the austenite matrix. A low ISFE promotes the presence of  $\epsilon$ -martensite, because an ISFE is in effect a thin nucleus of hcp  $\epsilon$ -martensite. Thicker  $\epsilon$ -martensite plates are formed by glide of Shockley partials  $1/6 \langle 112 \rangle_\gamma$  on every second  $\{111\}_\gamma$  plane, thereby forming an hcp region. In these alloys,  $\alpha'$ -martensite is formed at the intersection of two  $\epsilon$ -martensite laths or within an  $\epsilon$ -martensite lath. The ISFE, therefore, also plays a role, albeit indirectly, in the transformation of austenite into  $\alpha'$ -martensite in these alloys.<sup>[41,43,44]</sup>

The low strength of the austenite matrix implies that the strain-induced transformation will be easier, because, for the same stress level in the material, a higher strain is achieved. The grain size also influences the transformation, because a smaller grain size geometrically restricts the possibilities for the transformation to occur. In the case of the low Cr and med Cr alloys, the grain size of the hot-rolled annealed sample is smaller than the grain size of the N<sub>2</sub> annealed sample. Nevertheless, these alloys show more strain-induced transformation in the hot-rolled condition. This indicates that the influence of the matrix strength and that of the ISFE are more important than that of the grain size.

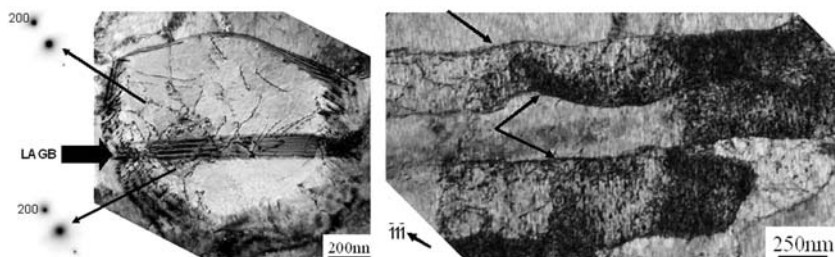


Fig. 9—TEM micrographs of the high Cr alloy, tested in tension in the hot-rolled and annealed condition. The microstructure is fully austenitic and contains dislocations ordered in low-angle grain boundaries (LAGBs) and cell structures, as indicated by the arrows.



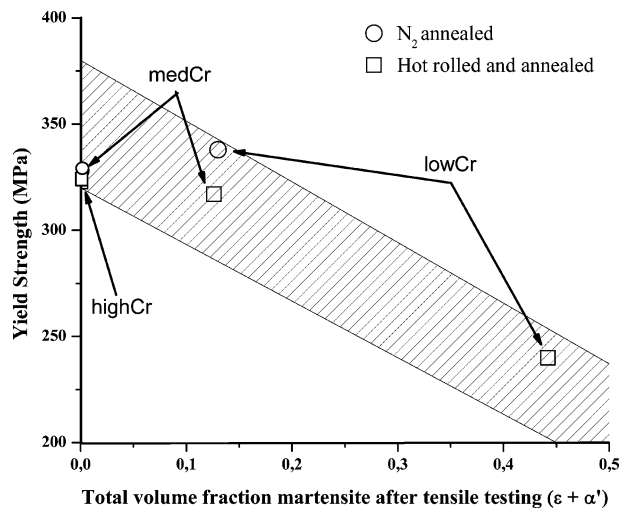


Fig. 11—Yield strength of the austenite matrix vs total amount of martensite formed during tensile testing: alloys with lower yield strength have a tendency to form higher amounts of  $\epsilon$ - and  $\alpha'$ -martensite during plastic deformation.

Considering that the  $\gamma \rightarrow \epsilon (\rightarrow \alpha')$  martensitic transformation requires a certain amount of plastic deformation in the steels studied, the yield strength of the materials can be used as a measure for the strength of the austenite matrix, because at the beginning of the deformation, no martensite will be present to harden the austenite. Figure 11 shows that samples with a higher yield strength have a tendency to undergo less strain-induced martensitic transformation than lower yield strength samples.

The second important influence on the transformation behavior is the ISFE of the alloy. It has been reported several times that increasing the ISFE of an austenitic alloy, by means of either the chemical composition or the test temperature, changes the deformation mode of the alloy,<sup>[13,15,20,36]</sup> as is shown schematically in Figure 12. This is in agreement with the results currently presented, because the low ISFE low Cr alloy deforms by strain-induced  $\gamma \rightarrow \epsilon \rightarrow \alpha'$  martensitic transformation and the higher ISFE high Cr alloy deforms by mechanical twinning. Based on this, it is obvious that the combined addition of Cr and N results in an increase of the ISFE for the alloys studied. The influence of Mn is expected to be limited in the chemical composition range studied. Further increasing the N content stabilized the austenite even more, indicating an increased ISFE for the  $N_2$  annealed samples. The increase of the ISFE with increasing amounts of Cr and N is in

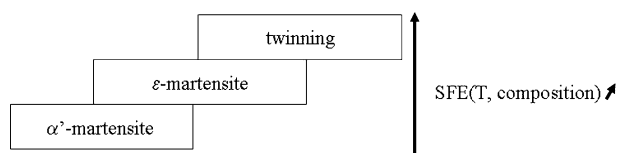


Fig. 12—Schematic representation of the ISFE dependency of the deformation mechanisms occurring in austenitic steels.

agreement with several results reported in the literature (refer to Section I).

Because the ISFE strongly influences the transformation behavior of austenitic steels, it seems logical that the mechanical properties are different as well. In a previous article,<sup>[44]</sup> it was illustrated that the low Cr in the hot-rolled and annealed condition does not show a beneficial transformation induced plasticity (TRIP) effect, contrary to what is commonly observed in Fe-Cr-Ni-based austenitic steels, *e.g.*, AISI 301. The latter have a sudden increase of strain hardening at a tensile strain of about 15 pct as a result of the strain-induced  $\gamma \rightarrow \alpha'$  martensitic transformation. The absence of this effect in the low Cr alloy in the hot-rolled and annealed condition was attributed to the fact that the  $\alpha'$ -martensite formed was restricted to the  $\epsilon$ -martensite lath within which it originated. Another important element that is important in obtaining a pronounced TRIP effect is the kinetics of the strain-induced martensitic transformation.<sup>[35,45]</sup> In the low Cr alloy in the hot-rolled and annealed condition, the kinetics is very fast, especially for the  $\gamma \rightarrow \epsilon$ -martensite transformation.<sup>[44]</sup> This is also reflected in the high strain-hardening value at low strains,  $n_{1-5}$ . Reducing the amount of  $\epsilon$ -martensite formed in the early stages of the deformation is expected to result in a better TRIP effect. For the low Cr alloy in the  $N_2$  annealed condition, the lower value of  $n_{1-5}$  indicates that the transformation kinetics is indeed slower as a consequence of the increased ISFE. However, the TRIP effect is still limited due to the too low amount of  $\alpha'$ -martensite formed in the later stages of deformation.

The med Cr deforms by  $\gamma \rightarrow \epsilon$ -martensitic transformation and mechanical twinning in the hot-rolled and annealed condition and by mechanical twinning in the  $N_2$  annealed condition, as does the high Cr in the hot-rolled and annealed condition. The fact that the last two do not form  $\epsilon$ -martensite results in a lower strain hardening, indicating that mechanical twins are less effective barriers for dislocation glide than  $\epsilon$ -martensite laths. The mechanical twins, however, are beneficial for elongation, as is clear from the results presented in Table II. The interface between the parent austenite and the  $\epsilon$ -martensite, *c.g.* mechanical twin, probably plays an important role in explaining these differences. The  $\epsilon$ -martensite phase has a slightly higher density than the parent austenite,<sup>[46]</sup> which causes coherency strains at the interface between the two phases. In the case of mechanical twins, these coherency strains do not exist, because the parent and the twinned austenite have the same crystal structure. The presence of coherency strains is expected to increase the interaction with slip dislocations, resulting in an increased strain hardening, on the one hand, but is expected to lead to earlier nucleation of microcracks and fracture, resulting in a lower elongation, on the other hand. Therefore, the alloys that deform by mechanical twinning have a superior ductility, and because they can be hardened up to higher strains, the tensile strength remains high.

The results presented show that alloy design based on the knowledge of the ISFE of an austenitic alloy can lead to the development of a steel with specific mechanical



properties through the control of the deformation mechanisms activated.

## V. CONCLUSIONS

The main conclusions of the present study are as follows.

1. Additions of Cr and N to a Fe-18Mn-0.25C austenitic steel resulted in a higher ductility and a more gradual strain-hardening behavior, which is beneficial for the deformation characteristics and for an increase of the potential of crash behavior.
2. Strain hardening is increased by the strain-induced martensitic  $\gamma \rightarrow \varepsilon$  ( $\rightarrow \alpha'$ ) transformation and mechanical twinning. The effect of the strain-induced transformation was stronger than the effect of twinning, indicating that twin boundaries are less effective as a barrier for dislocation glide than  $\varepsilon$ -martensite phase boundaries. Twinning, however, is beneficial for ductility.
3. Increasing the N content up to 0.22 mass pct improves ductility and reduces strain hardening, which is beneficial for applications where a high energy absorption potential is required, e.g., for passive safety related parts in the automotive industry. As a result, the best energy absorption properties were achieved for the Fe-19Mn-0.24C-9.7Cr-0.196N and the Fe-19Mn-0.24C-7.7Cr-0.196N alloys.
4. The Cr and N additions to a Fe-18Mn-5.6Cr-0.25C alloy increase the ISFE, resulting in a suppression of strain-induced martensitic  $\gamma \rightarrow \varepsilon$  ( $\rightarrow \alpha'$ ) transformation.

## ACKNOWLEDGMENT

The authors acknowledge ir. G. Lannoo, Product Technology Department of CRM, for performing the hot rolling.

## REFERENCES

1. B.R. Nijhawan, P.K. Gupte, S.S. Bhatganar, B.K. Guha, and S.S. Dhanjal: *J. Iron Steel Inst.*, 1967, Mar., pp. 292–304.
2. B.D. Shanina, V.G. Gavriljuk, H. Berns, and F. Schmalz: *Steel Res.*, 2002, vol. 73 (3), pp. 105–13.
3. G. Balachandran, M.L. Bhatia, N.B. Ballal, and P. Krishna Rao: *ISIJ Int.*, 2001, vol. 41 (9), pp. 1018–27.
4. S.R. Chen, H.A. Davies, and W.M. Rainforth: *Acta Mater.*, 1999, vol. 47 (18), pp. 4555–69.
5. R. Franks, W.O. Binder, and J. Thompson: *Trans. ASM*, 1955, vol. 47, pp. 231–64.
6. G. Frommeyer, U. Brück, and P. Neumann: *ISIJ Int.*, 2003, vol. 43 (3), pp. 438–46.
7. S. Allain, J.-P. Chateau, and O. Bouaziz: *Steel Res.*, 2002, vol. 73 (6–7), pp. 299–302.
8. S. Vercammen, B. Blanpain, B.C. De Cooman, and P. Wollants: *Acta Mater.*, 2004, vol. 52, pp. 2005–12.
9. K. Ishida and T. Nishizawa: *Trans. JIM*, 1974, vol. 15, pp. 225–31.
10. P.M. Gilles and A.R. Marder: *Metall. Trans.*, 1971, vol. 2, pp. 1371–78.
11. N. Cabañas-Poy: Ph.D. Thesis, Ghent University, Zwijnaarde, Belgium, 2004.
12. J.P. Hirth: *Metall. Trans.*, 1970, vol. 1, pp. 2367–74.
13. S. Allain, J.-P. Chateau, O. Bouaziz, S. Migot, and N. Guelton: *Mater. Sci. Eng. A*, 2004, vols. 387–389, pp. 158–62.
14. H. Schumann: *Neue Hütte*, 1972, vol. 17, pp. 605–09.
15. K. Sato, M. Ichinose, Y. Hirotsu, and Y. Inoue: *ISIJ Int.*, 1989, vol. 29 (10), pp. 868–77.
16. I.V. Kireeva, N.V. Luzginova, Y.I. Chumlyakov, and I. Karaman: *J. Phys. IV*, 2004, vol. 115, pp. 223–30.
17. R.E. Stoltz and J.B. Vander Sande: *Metall. Trans. A*, 1980, vol. 11A, pp. 1033–37.
18. I.A. Yakubtsov, A. Ariapour, and D.D. Perovic: *Mater. Sci. Forum*, 1999, vols. 318–320, pp. 121–30.
19. I.A. Yakubtsov, A. Ariapour, and D.D. Perovic: *Acta Mater.*, 1999, vol. 47 (4), pp. 1271–79.
20. I. Karaman, H. Sehitoglu, H.J. Maier, and Y.I. Chumlyakov: *Acta Mater.*, 2001, vol. 49, pp. 3919–33.
21. V.G. Gavriljuk, H. Berns, C. Escher, N.I. Glavatskaya, A. Sozinov, and Y.N. Petrov: *Mater. Sci. Eng. A*, 1999, vol. 271, pp. 14–21.
22. J. Wan, X. Huang, S. Chen, and T.Y. Hsu (Xu Zuyao): *Mater. Trans.*, 2002, vol. 43 (5), pp. 920–25.
23. B. Jiang, X. Qi, S. Yang, W. Zhou, and T.Y. Hsu: *Acta Mater.*, 1998, vol. 46 (2), pp. 501–10.
24. V.G. Gavriljuk, A.L. Sozinov, J. Foct, J.N. Petrov, and Y.A. Polushkin: *Acta Mater.*, 1998, vol. 46 (4), pp. 1157–63.
25. C.G. Rhodes and A.W. Thompson: *Metall. Trans. A*, 1977, vol. 8A, pp. 1901–06.
26. R.E. Schramm and P. Reed: *Metall. Trans. A*, 1975, vol. 6A, pp. 1345–51.
27. Y. Ustinovshokov, A. Ruts, O. Bannykh, V. Blinov, and M. Kostina: *Mater. Sci. Eng. A*, 1999, vol. 262, pp. 82–87.
28. J.W. Simmons: *Acta Mater.*, 1997, vol. 45 (6), pp. 2467–75.
29. G. Balachandran, M.L. Bhatia, N.B. Ballal, and P. Krishna Rao: *ISIJ Int.*, 2000, vol. 40 (5), pp. 501–10.
30. V.G. Gavriljuk, H. Berns, C. Escher, N.I. Glavatskaya, A. Sozinov, and Y.N. Petrov: *Mater. Sci. Eng. A*, 1999, vol. 271, pp. 14–21.
31. M.O. Speidel and M. Zheng-Cui: *Proc. 6th Int. Conf. on High Nitrogen Steels HNS2003*, Vdf Hochschulverlag, Zürich, Feb. 2003, pp. 63–73.
32. V.G. Gavriljuk: *ISIJ Int.*, 1996, vol. 36 (7), pp. 738–45.
33. V.G. Gavriljuk, B.D. Shanina, and H. Berns: *Acta Mater.*, 2000, vol. 48, pp. 3879–93.
34. G.B. Olson and M. Cohen: *Metall. Trans. A*, 1975, vol. 6A, pp. 791–95.
35. O. Grässel, G. Frommeyer, and L.W. Meyer: *Int. J. Plast.*, 2000, vol. 16, pp. 1391–1409.
36. L. Remy and A. Pineau: *Mater. Sci. Eng.*, 1977, vol. 28, p. 99.
37. T. Tsuchiyama, H. Ito, K. Katakao, and S. Takaki: *Metall. Mater. Trans. A*, 2003, vol. 34A, pp. 2591–99.
38. M. De Meyer, D. Vanderschueren, K. De Blauwe, and B.C. De Cooman: *41st MWSP Conf. Proc.*, ISS, Warrendale, PA, 1999, vol. 37, pp. 483–92.
39. J.C. Li, W. Zheng, and Q. Jiang: *Mater. Lett.*, 1999, vol. 38, pp. 275–77.
40. P. Marshall: *Austenitic Stainless Steels*, Elsevier Applied Science Publishers, London, 1984, p. 81.
41. L. Bracke, M. Liebeherr, N. Akdut, and B.C. De Cooman: *Proc. 7th Int. Conf. on High Nitrogen Steels HNS2004*, Ostend, Belgium, Sept 2004, GRIPS Media GmbH, Bad Harzburg, Germany Bad Harzburg, 2004, pp. 331–41.
42. G.B. Olson and M. Cohen: *J. Less-Common Met.*, 1972, vol. 28, pp. 107–18.
43. A.J. Bogers and W.G. Burgers: *Acta Metall.*, 1964, vol. 12, pp. 255–61.
44. L. Bracke, G. Mertens, J. Penning, B.C. De Cooman, M. Liebeherr, and N. Akdut: *Mater. Trans. A*, 2006, vol. 37A, pp. 307–17.
45. P.C. Maxwell, A. Goldberg, and J.C. Shyne: *Metall. Trans.*, 1974, vol. 5A, pp. 1319–24.
46. J.W. Brooks, M.H. Loretto, and R.E. Smallman: *Acta Metall.*, 1979, vol. 27, pp. 1839–47.